

# New family of $\text{Ln}_9\text{Mn}_4$ ( $\text{Ln} = \text{Gd}, \text{Tb}, \text{Dy}$ ) and $\text{Y}_9\text{Mn}_4$ clusters from the use of methyl-2-pyridyl-ketone oxime in heterometallic Mn chemistry<sup>\*</sup>

Linh Pham<sup>a,b</sup>, Thai Son Cao<sup>a</sup>, Khalil A. Abboud<sup>a</sup>, George Christou<sup>a,\*</sup>

<sup>a</sup> Department of Chemistry, University of Florida, Gainesville, FL 32611-7200, USA

<sup>b</sup> Department of Science and Mathematics, Texas A&M University-Central Texas, Killeen, TX 76549, USA

## ARTICLE INFO

### Keywords:

Crystal structure  
Manganese  
Lanthanides  
Clusters  
Magnetic properties

## ABSTRACT

A new family of  $[\text{Ln}_9\text{Mn}_4\text{O}_8(\text{OH})_4(\text{O}_2\text{CPh})_{17}(\text{mpko})_4]$  ( $\text{Ln}^{\text{III}} = \text{Gd}$  (**2**),  $\text{Tb}$  (**3**),  $\text{Dy}$  (**4**);  $2\text{Mn}^{\text{III}}$ ,  $2\text{Mn}^{\text{IV}}$ ) clusters and their diamagnetic  $\text{Y}^{\text{III}}$  analog (**1**) have been obtained from the reaction of  $\text{Mn}(\text{O}_2\text{CPh})_2$ ,  $\text{LnCl}_3$  or  $\text{YCl}_3$ , methyl-2-pyridyl-ketone oxime (mpkoH), and  $\text{NMe}_4\text{OH}$  in a 2:2:2:4 M ratio in  $\text{MeCN}/\text{CH}_2\text{Cl}_2$  (22:3 mL). The crystal structure of  $4\text{-CH}_2\text{Cl}_2\text{-8MeCN}$  reveals a very low-symmetry core comprising a  $[\text{Dy}_2\text{Mn}_2\text{O}_4]$  cubane sandwiched between a  $\{\text{Dy}_7\text{MnO}_4(\text{OH})_4\}$  unit and an external Mn atom; alternatively, it can be described as a zig-zag 1-D  $\{\text{Mn}^{\text{IV}}\text{OMn}^{\text{IV}}\text{O}_2\text{Mn}^{\text{III}}\text{OMn}^{\text{III}}\}_{6+}$  unit sandwiched between  $\text{Dy}_5$  and  $\text{Dy}_4$  units. Fitting of the variable-temperature, solid-state dc and ac magnetic susceptibility data on the  $\text{Mn}_4$  unit of **1** revealed dominant anti-ferromagnetic (AF) Mn...Mn interactions:  $J_1 = -22.5(9) \text{ cm}^{-1}$ ,  $J_2 = -7.6(5) \text{ cm}^{-1}$ , and  $J_3 = +0.30(3) \text{ cm}^{-1}$ , with a constant  $g = 1.97$ , where  $J_1$ ,  $J_2$ , and  $J_3$  are the  $J(\text{Mn}^{\text{IV}}\text{Mn}^{\text{IV}})$ ,  $J(\text{Mn}^{\text{IV}}\text{Mn}^{\text{III}})$ , and  $J(\text{Mn}^{\text{III}}\text{Mn}^{\text{III}})$  exchange parameters, respectively. These parameters indicate an  $S = 4$  ground state with  $S_T = 3$  and  $S_T = 2$  excited states at 2.4 and 4.2  $\text{cm}^{-1}$ , respectively, above it. The many non-equivalent Mn...Gd interactions in  $\text{Gd}_9\text{Mn}_4$  complex **2** were deduced to include both F and AF interactions leading to an  $S = 18$  or 19 ground state. Complexes **3** and **4** exhibited frequency-dependent ac out-of-phase ( $\chi''_M$ ) signals below 4 K indicating them to be weak SMMs.

## 1. Introduction

Since the publication of the  $\text{Tb}_2\text{Cu}_2$  single-molecule magnet (SMM) in 2004 [1], 3d-4f metal-oxo coordination clusters have attracted intense interest from the molecular magnetism community and have been a rich source of new SMMs, as well as clusters with fascinating and aesthetically pleasing structures, owing to the high anisotropy of lanthanide (Ln) ions and their often ferromagnetic coupling with 3d transition metals [2-18]. For example, a  $\text{DyCo}_2$  complex with the  $\text{Dy}^{\text{III}}$  adopting near-trigonal bipyramidal ( $D_{5h}$ ) geometry symmetry holds the record for the highest energy barrier in 3d-4f SMMs with  $U_{\text{eff}} = 416 \text{ cm}^{-1}$  [19]. Many Mn-based homo- or heterometallic 3d-4f SMMs with significant relaxation barriers are composed of either  $\text{Mn}^{\text{III}}_x$  or mixed-valent  $\text{Mn}^{\text{III}}/\text{Mn}^{\text{IV}}$  species including  $\text{Mn}_4$  [20],  $\text{Mn}_6$  [21],  $\text{Mn}_{25}$  [22],  $\text{Mn}_{26}$  [23],  $\text{Mn}_{84}$  [24],  $\text{Mn}_2\text{Dy}$  [6],  $\text{Mn}_4\text{Tb}_2$  [25],  $\text{Mn}_4\text{Dy}_4$  [26],  $[\text{Mn}_7\text{Er}]$  [27],  $\text{Mn}_{11}\text{Dy}_4$  [28],  $\text{Mn}_6\text{Dy}_6$  [29],  $\text{Mn}_{11}\text{Gd}_2$  [30],  $\text{Mn}_{12}\text{Gd}$  [31],  $\text{Mn}_{18}\text{Dy}$  [32],  $\text{Mn}_{21}\text{Dy}$  [33],  $\text{Mn}_{12}\text{Ln}_6$  [34],  $\text{Mn}_8\text{Dy}_4$  [35], and  $\text{Mn}_{16}\text{Dy}_2$  [36]. The giant, torus-shaped  $\text{Mn}_{84}$  [24] and  $\text{Mn}_{70}$  [37] SMMs with a  $\sim 4 \text{ nm}$  size also 'straddle the classical/quantum interface' with magnetic

properties that can be analyzed by both quantum and classical methods. The development of various synthetic methods has supported the progress in Mn-based 3d-4f magnetic clusters, including compartmentalized ligands, assisted self-assembly, comproportionation, reductive aggregation, and others [38-41]. However, the structures of many 3d-4f SMMs reported so far could not have been accurately predicted because 3d and 4f metal ions prefer different coordination geometries, but once a product has been identified it is almost always possible to expand it into a family by changes in the 4f metal to vary the anisotropy or to replace it with the diamagnetic  $\text{Ln}^{\text{III}}$  or non-Ln  $\text{Y}^{\text{III}}$  [42,43].

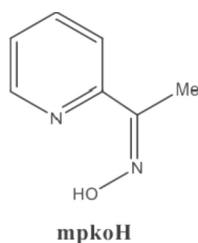
In the past two decades, pyridyl oximes have been intensively investigated in coordination chemistry because of their versatile ligation as chelating and bridging ligands, which yield numerous compounds with fascinating structures and intriguing electronic and magnetic properties [44-52]. For example, methyl-2-pyridyl-ketone oxime (mpkoH) when deprotonated becomes a versatile bridging/chelating oximate that has facilitated the synthesis of a variety of fascinating high-nuclearity 3d and 3d-4f clusters [53-58] and also been found to promote strong ferromagnetic (F) couplings between Mn centers [59]. Our own

<sup>\*</sup> Part of the special issue dedicated to the element manganese, entitled *Manganese: A Tribute to Chemical Diversity*

<sup>\*</sup> Corresponding author.

E-mail address: [christou@chem.ufl.edu](mailto:christou@chem.ufl.edu) (G. Christou).

group has taken advantage of this chemistry, namely the triangular  $[\text{Mn}_3\text{O}(\text{O}_2\text{CR})_3(\text{mpko})_3]^+$  SMM cation with an  $S = 6$  ground state, to develop



routes to a family of covalently-connected  $[\text{Mn}_3]_n$  ( $n = 2, 4$ ) supra-molecular oligomers linked together by replacing the mpko<sup>-</sup> groups with dioximates [60], or the carboxylates with dicarboxylates [61]. In addition, we have employed mpkoH in a number of other reaction systems, with either carboxylate or phosphorus-based ancillary ligands such as phosphinates or phosphonates [58,62,63]. We herein report the results from one such investigation, the syntheses, crystal structure, and magnetochemical characterization of a new family of low-symmetry  $\text{Ln}_n\text{Mn}_4$  and  $\text{Y}_9\text{Mn}_4$  clusters with mpko<sup>-</sup> as the key bridging and chelating ligand.

## 2. Experimental

### 2.1. Syntheses

All procedures were carried out under aerobic conditions and at ambient conditions of temperature and light. The synthesis of mpkoH was conducted as previously reported [48]. All chemicals were used as received.

#### 2.1.1. $[\text{Y}_9\text{Mn}_4\text{O}_8(\text{OH})_4(\text{O}_2\text{CPh})_{17}(\text{mpko})_4]$ (1)

To a stirred solution of mpkoH (0.24 g, 2.0 mmol) in MeCN/ $\text{CH}_2\text{Cl}_2$  (22/3 mL) was added  $\text{YCl}_3 \cdot 6\text{H}_2\text{O}$  (0.61 g, 2.0 mmol) followed by the addition of a solution of  $\text{NMe}_4\text{OH}$  (316  $\mu\text{L}$ , 4.0 mmol) in MeOH. After stirring for 10 min,  $\text{Mn}(\text{O}_2\text{CPh})_2 \cdot 4\text{H}_2\text{O}$  (0.74 g, 2.0 mmol) was introduced and the resulting dark brown solution stirred for six hours. It was then filtered to remove any undissolved solid and the filtrate maintained undisturbed at ambient temperature with slight concentration of the mother liquor by slow evaporation. Dark brown, plate-like crystals slowly grew over the course of one week, and these were collected by filtration, washed with  $\text{Et}_2\text{O}$ , and dried under vacuum for 3 h. The yield was 25% based on Mn. Anal. Calcd. (Found) for  $1 \cdot \text{H}_2\text{O}$  ( $\text{C}_{147}\text{H}_{119}\text{Y}_9\text{Mn}_4\text{N}_8\text{O}_{51}$ ): C, 46.06 (46.03); H, 3.13 (3.41); N, 2.92 (2.89)%. Selected IR data (KBr,  $\text{cm}^{-1}$ ): 3426(br), 3063(m), 1600(s), 1557(s), 1419(s), 1306(w), 1176(m), 1025(m), 963(w), 778(m), 718(s), 689(w), 672(w), 642(m), 562(w), 428(s). The IR spectra of the other compounds are essentially superimposable.

#### 2.1.2. $[\text{Gd}_9\text{Mn}_4\text{O}_8(\text{OH})_4(\text{O}_2\text{CPh})_{17}(\text{mpko})_4]$ (2)

The preparation of **2** was similar to that for **1**, but with  $\text{GdCl}_3 \cdot 6\text{H}_2\text{O}$  (0.74 g, 2.0 mmol). The yield was 34% based on Mn. Calcd. (Found) for  $2 \cdot \text{H}_2\text{O}$  ( $\text{C}_{147}\text{H}_{119}\text{Gd}_9\text{Mn}_4\text{N}_8\text{O}_{51}$ ): C, 39.69 (39.57); H, 2.70 (2.54); N, 2.52 (2.39)%.

#### 2.1.3. $[\text{Tb}_9\text{Mn}_4\text{O}_8(\text{OH})_4(\text{O}_2\text{CPh})_{17}(\text{mpko})_4]$ (3)

The preparation of **3** was similar to that for **1**, but with  $\text{TbCl}_3 \cdot 6\text{H}_2\text{O}$  (0.75 g, 2.0 mmol). The yield was 36% based on Mn. Anal. Calcd. (Found) for  $3 \cdot \text{H}_2\text{O}$ : ( $\text{C}_{147}\text{H}_{119}\text{Tb}_9\text{Mn}_4\text{N}_8\text{O}_{51}$ ): C, 39.56 (39.40); H, 2.69 (2.43); N, 2.51 (2.34)%.

#### 2.1.4. $[\text{Dy}_9\text{Mn}_4\text{O}_8(\text{OH})_4(\text{O}_2\text{CPh})_{17}(\text{mpko})_4]$ (4)

The preparation of **4** was similar to that for **1**, but with  $\text{DyCl}_3 \cdot 6\text{H}_2\text{O}$  (0.75 g, 2.0 mmol). The yield of  $4 \cdot \text{CH}_2\text{Cl}_2 \cdot 8\text{MeCN}$  was 35% based on Mn; the crystals for X-ray studies were maintained in mother liquor to avoid

**Table 1**

Crystallographic and structure refinement data for  $4 \cdot \text{CH}_2\text{Cl}_2 \cdot 8\text{MeCN}$ .

Parameter	$4 \cdot \text{CH}_2\text{Cl}_2 \cdot 8\text{MeCN}$
Formula	$\text{C}_{164}\text{H}_{143}\text{Cl}_2\text{Dy}_9\text{Mn}_4\text{N}_{16}\text{O}_{50}$
fw, g mol <sup>-1a</sup>	4891.09
crystal system	Triclinic
space group	$P\bar{1}$
<i>a</i> , Å	17.4023(4)
<i>b</i> , Å	17.6496(4)
<i>c</i> , Å	28.9205(6)
$\alpha$ , deg	73.2214(13)
$\beta$ , deg	88.3318(12)
$\gamma$ , deg	87.1559(13)
<i>V</i> , Å <sup>3</sup>	8493.1(3)
<i>Z</i>	2
<i>T</i> , °K	100(2)
radiation, Å <sup>b</sup>	0.71073
$\rho_{\text{calc}}$ , g cm <sup>-3</sup>	1.911
$\mu$ , mm <sup>-1</sup>	24.090
$R_1^c$	0.0889
$wR_2^d$	0.2055

<sup>a</sup> Including solvent molecules.

<sup>b</sup>  $I > 2\sigma(I)$ .

<sup>c</sup>  $R_1 = \sum(|F_o| - |F_c|) / \sum|F_o|$

<sup>d</sup>  $wR_2 = [\sum[w(F_o^2 - F_c^2)^2] / \sum[w(F_o^2)^2]]^{1/2}$ ;  $w = 1/[\sigma^2(F_o^2) + (m^*p)^2 + n^*p]$ ,  $p = [\max(F_o^2, 0) + 2^*F_c^2]/3$ , *m* and *n* are constants.

degradation through solvent loss. Anal. Calcd. (Found) for  $4 \cdot \text{H}_2\text{O}$  ( $\text{C}_{147}\text{H}_{119}\text{Dy}_9\text{Mn}_4\text{N}_8\text{O}_{51}$ ): C, 39.27 (39.37); H, 2.67 (2.44); N, 2.49 (2.37)%.

### 2.2. X-ray crystallography

A suitable single crystal of  $4 \cdot \text{CH}_2\text{Cl}_2 \cdot 8\text{MeCN}$  was attached to a glass fiber using silicone grease and transferred to the goniostat where it was cooled to 100 K for characterization and data collection on a Bruker DUO diffractometer using  $\text{CuK}\alpha$  radiation ( $\lambda = 1.54178$  Å), from an  $\mu\text{S}$  power source, and an APEXII CCD area detector. Raw data frames were read by program SAINT [64] and integrated using 3D profiling algorithms. The resulting data were reduced to produce hkl reflections and their intensities and estimated standard deviations. The data were corrected for Lorentz and polarization effects and numerical absorption corrections were applied based on indexed and measured faces. The structure was solved and refined in SHELXTL2013 [65] using full-matrix least-squares cycles. The non-H atoms were refined with anisotropic thermal parameters, whereas all of the H atoms were placed in calculated, idealized positions and refined as riding on their parent atoms.

The asymmetric unit consists of the complete  $\text{Dy}_9\text{Mn}_4$  cluster, and one  $\text{CH}_2\text{Cl}_2$  and eight MeCN solvent molecules. The solvent molecules were disordered and could not be modeled properly, thus program SQUEEZE [65], a part of the PLATON [65] package of crystallographic software, was used to calculate the solvent disorder area and remove its contribution to the overall intensity data. There are four Ph groups that were disordered and each was refined in two parts with their site occupation factors fixed at a ratio of 60/40 for the C121, C161, C171 and 50/50 for the C201 group. These Ph groups were also idealized using "AFIX 66" in the refinement of the final model. Inspection of the packing reveals that the solvents are scattered in voids in the packing and are also close to the disordered Ph rings. In the final cycle of refinement, 29,350 reflections (of which 22,553 are observed with  $I > 2\sigma(I)$ ) were used to refine 1831 parameters and the resulting  $R_1$ ,  $wR_2$  and *S* (goodness of fit) were 7.29%, 19.16% and 1.094, respectively. The refinement was carried out by minimizing the  $wR_2$  function using  $F^2$  rather than *F* values.  $R_1$  is calculated to provide a reference to the conventional R value but its function is not minimized. Unit cell data and structure refinement details are collected in Table 1.

**Table 2**  
Selected interatomic distances (Å) and angles (deg) for 4.

Mn(1)-O(5)	1.853(7)	Mn(3)-O(3)	1.846(6)
Mn(1)-O(1)	1.867(7)	Mn(3)-O(12)	1.855(6)
Mn(1)-O(7)	1.879(6)	Mn(3)-O(7)	1.868(7)
Mn(1)-O(11)	1.935(7)	Mn(3)-O(10)	1.887(7)
Mn(1)-O(16)	1.973(7)	Mn(3)-O(15)	1.987(6)
Mn(1)-O(4)	1.978(7)	Mn(4)-O(3)	1.925(6)
Mn(2)-O(9)	1.811(7)	Mn(4)-O(12)	1.932(7)
Mn(2)-O(22)	1.999(8)	Mn(4)-O(13)	1.947(7)
Mn(2)-O(19)	2.116(7) <sup>a</sup>	Mn(4)-O(23)	1.954(7)
Mn(2)-O(17)	2.380(7) <sup>a</sup>	Mn(4)-O(9)	2.122(7) <sup>a</sup>
Mn(3)-O(2)	1.841(7)	Mn(4)-O(14)	2.125(8) <sup>a</sup>
Mn(3)-O(3)-Mn(4)	96.0(3) <sup>b</sup>	Mn(1)-O(7)-Mn(3)	129.1(3)
Mn(3)-O(12)-Mn(4)	95.4(3) <sup>b</sup>	Mn(2)-O(9)-Mn(4)	116.1(3)

<sup>a</sup> Jahn-Teller elongation axes.

<sup>b</sup> Angles within the {Dy<sub>2</sub>Mn<sub>2</sub>O<sub>4</sub>} cube.

### 2.3. Physical measurements

Infrared spectra in the 400–4000 cm<sup>-1</sup> range were recorded in the solid state (KBr pellets) on a Nicolet Nexus 670 FTIR spectrometer.

Elemental analyses (C, H and N) were performed by the in-house facilities of the University of Florida Chemistry Department. Variable-temperature dc and ac magnetic susceptibility data were collected on a Quantum Design MPMS-XL SQUID magnetometer equipped with a 7 T magnet and operating in the 1.8–300 K range. Samples were embedded in solid eicosane to prevent torquing. Magnetization vs dc field and temperature data were fit using the program MAGNET [66]. Pascal's constants were used to estimate the diamagnetic corrections, and a blank with just eicosane was measured to determine its diamagnetism, which were subtracted from the experimental susceptibilities to give the molar paramagnetic susceptibilities ( $\chi_M$ ).

## 3. Results and discussion

### 3.1. Syntheses

The oxidation of Mn<sup>II</sup> benzoate by atmospheric O<sub>2</sub> in the presence of LnCl<sub>3</sub> (Ln = Gd, Tb, Dy) or YCl<sub>3</sub>, mpkoH, and NMe<sub>4</sub>OH in a 2:2:2:4 M ratio in MeCN/CH<sub>2</sub>Cl<sub>2</sub> (22/3 mL) led to dark brown solutions from which were isolated dark brown plate-like crystals of the corresponding

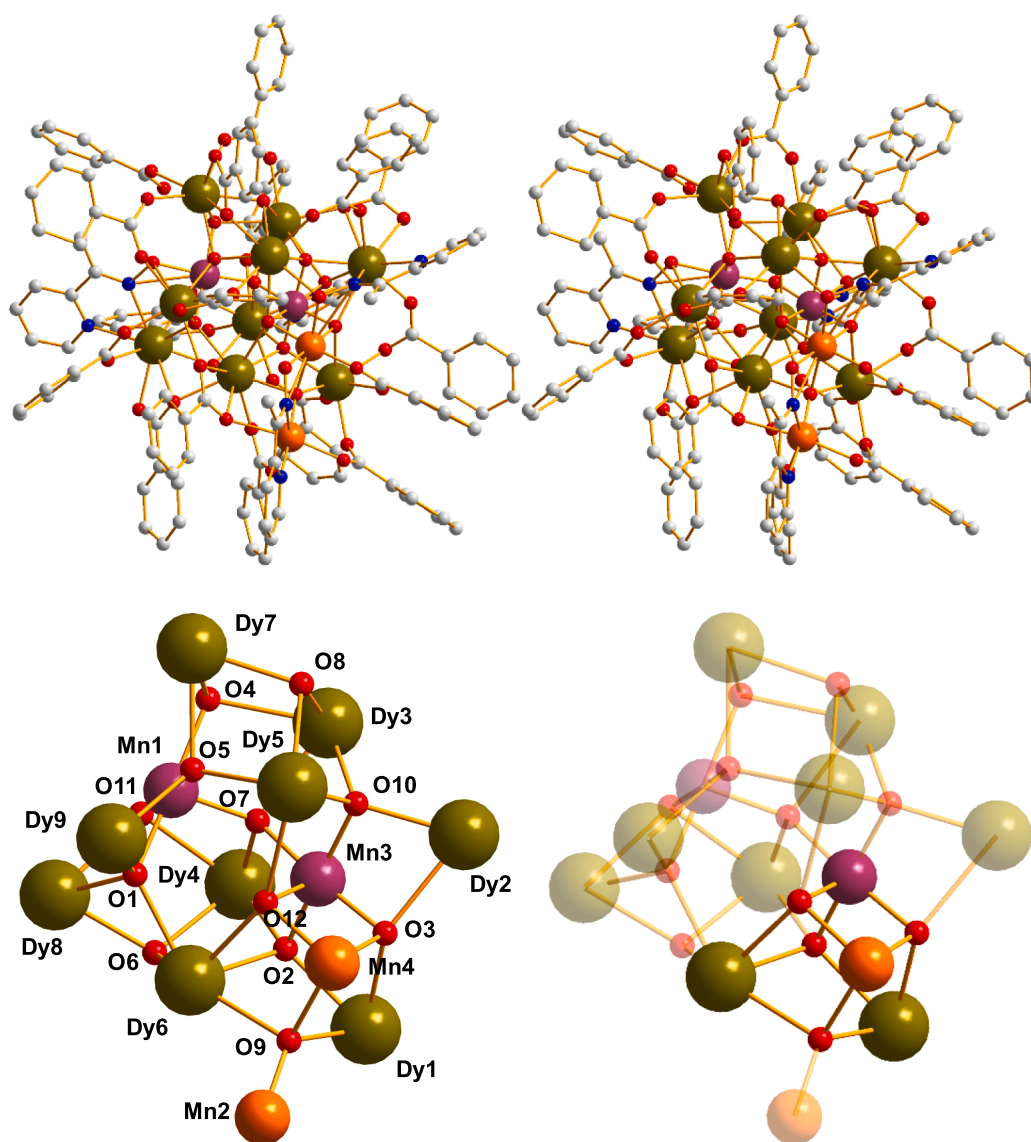


**Fig. 1.** (top) Stereopair of the complete structure of 4, except that H atoms have been omitted for clarity; and (bottom) its labeled core and a view emphasizing the location of the {Dy<sub>2</sub>Mn<sub>2</sub>O<sub>4</sub>} cubane. Color code: Dy green, Mn<sup>III</sup> orange, Mn<sup>IV</sup> purple, O red, N blue, C grey.

**Table 3**  
BVS values for the Mn<sup>a</sup> and selected O atoms<sup>b</sup> of **4**.

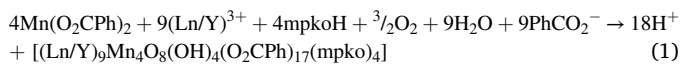
Atom	Mn <sup>II</sup>	Mn <sup>III</sup>	Mn <sup>IV</sup>
Mn1	4.04	3.69	<u>3.88</u>
Mn2	3.06	<u>2.86</u>	2.91
Mn3	4.42	4.04	<u>4.25</u>
Mn4	3.25	<u>2.97</u>	3.12
Atom	BVS	Assigned	
O1	1.94	$\mu_4\text{-O}^{2-}$	
O2	1.98	$\mu_4\text{-O}^{2-}$	
O3	1.93	$\mu_4\text{-O}^{2-}$	
O4	1.23	$\mu_3\text{-OH}^-$	
O5	1.96	$\mu_4\text{-O}^{2-}$	
O6	1.20	$\mu_3\text{-OH}^-$	
O7	2.07	$\mu_4\text{-O}^{2-}$	
O8	1.26	$\mu_3\text{-OH}^-$	
O9	1.86	$\mu_4\text{-O}^{2-}$	
O10	2.24	$\mu_4\text{-O}^{2-}$	
O11	1.18	$\mu_3\text{-OH}^-$	
O12	1.74	$\mu_4\text{-O}^{2-}$	

which is the closest to the charge for which it was calculated.

For O, values of 0.8–1.2 and 1.8–2.2 are typical for OH<sup>-</sup> and O<sup>2-</sup> ions, respectively.

<sup>a</sup> For Mn, the oxidation state is the nearest integer to the underlined value,

[(Ln/Y)<sub>9</sub>Mn<sub>4</sub>O<sub>8</sub>(OH)<sub>4</sub>(O<sub>2</sub>CPh)<sub>17</sub>(mpko)<sub>4</sub>] (2Mn<sup>III</sup>, 2Mn<sup>IV</sup>) clusters in 25–35% non-optimized yields based on Ln/Y (Eq. (1)). If the CH<sub>2</sub>Cl<sub>2</sub> was omitted the same products were obtained as powders rather than crystals. The NMe<sub>4</sub>OH, a strong base, was used to facilitate Mn<sup>II</sup> oxidation by O<sub>2</sub> and provide additional H<sup>+</sup> acceptors. The essentially superimposable IR spectra, the elemental analysis data, and the similar magnetic data indicated **1–4** to be isostructural.



### 3.2. Description of the structure

The complete structure of **4** as a stereopair and its core are shown in Fig. 1. Selected bond distances and angles are listed in Table 2. The {Dy<sub>9</sub>Mn<sub>4</sub>( $\mu_4\text{-O}$ )<sub>8</sub>( $\mu_3\text{-OH}$ )<sub>4</sub>} core is very low symmetry and is unprecedented within 3d-4f chemistry. It can be described as a central {Mn<sub>2</sub>Dy<sub>2</sub>O<sub>4</sub>} cubane (Mn3, Mn4, Dy1, Dy6) with one of its oxide ions

attached to external Mn2 on one side, while on the other side the other three cubane oxides are each bound to a Dy ion of a low symmetry {Dy<sub>7</sub>MnO<sub>4</sub>(OH)<sub>4</sub>} unit (Fig. 1, bottom). Alternatively, it can be described as a zig-zag Mn<sub>4</sub> unit sandwiched between Dy<sub>4</sub> and Dy<sub>5</sub> units. The Mn oxidation states were confirmed to be 2Mn<sup>III</sup> and 2Mn<sup>IV</sup> by bond valence sum (BVS) calculations (Table 3) [67,68], with one of each in the {Mn<sub>2</sub>Dy<sub>2</sub>O<sub>4</sub>} cubane. The four mpko<sup>-</sup> chelates exhibit three different ligation modes bridging two, three and four metals (Scheme), the  $\mu_3$  mode occurring twice. Other oximate binding modes seen in the literature include  $\eta^1$  [69],  $\eta^2$  [70],  $\eta^1:\eta^1:\mu$  [71],  $\eta^1:\eta^1:\eta^1:\mu$  [72], and  $\eta^1:\eta^2:\eta^1:\mu_3$  [73]. Ligation is completed by seventeen benzoate groups in four binding modes ranging from monodentate  $\eta^1$  to a very unusual  $\eta^2:\eta^2:\mu_3$  mode (Scheme 1). The unbound O46 of the  $\eta^1$  benzoate

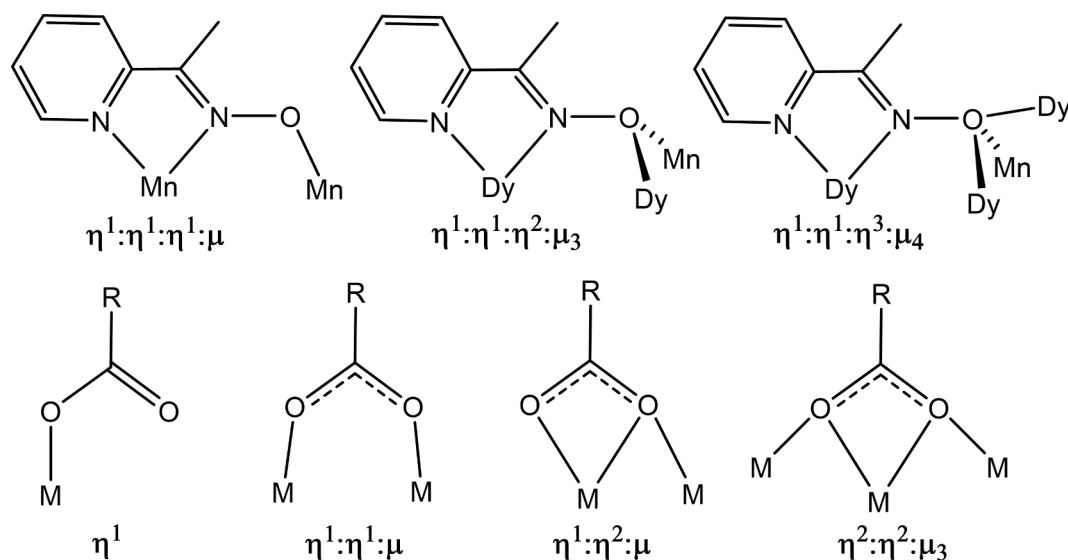
forms an internal hydrogen-bond with the  $\mu_3\text{-OH}^-$  atom O4 (O4...O46 = 2.590(9) Å). The two Mn<sup>III</sup> ions, Mn2 and Mn4, possess near-octahedral geometries and resultant Jahn-Teller axial elongations that coincide with the Mn2-O17, Mn2-O19, Mn4-O14 and Mn4-O9 bonds (Table 2). The first three are bonds to benzoate or oximate O atoms, but the last (Mn4-O9 = 2.122(7) Å) is to an O<sup>2-</sup> ion of the {Mn<sub>2</sub>Dy<sub>2</sub>O<sub>4</sub>} cubane and is significantly longer than the other two Mn4-O<sup>2-</sup> bonds within the cubane (Mn4-O3 = 1.925(6) and Mn4-O12 = 1.932(6) Å). Examination of the packing of the molecules reveals intermolecular  $\pi\text{-}\pi$  stacking between the pyridyl ring of an mpko<sup>-</sup> ligand chelating Mn2 and bridging to Mn4, and a benzoate bridging two Dy<sup>III</sup> atoms (closest C...C = 3.279 Å) on the adjacent molecule, giving a chain.

### 3.3. Magnetochemistry

#### 3.3.1. Dc magnetic susceptibility studies

Solid-state, variable-temperature magnetic susceptibility ( $\chi_M$ ) measurements were performed on powdered microcrystalline samples of vacuum-dried 1·H<sub>2</sub>O - 4·H<sub>2</sub>O, restrained in eicosane to prevent torquing, in the 5.0–300 K range and in a 1 kG (0.1 T) dc field. The obtained data are plotted as  $\chi_M T$  vs  $T$ .

For Y<sub>9</sub>Mn<sub>4</sub> compound 1·H<sub>2</sub>O, containing diamagnetic Y<sup>III</sup> ions,  $\chi_M T$  decreases from 8.52 cm<sup>3</sup> K mol<sup>-1</sup> at 300 K to a minimum of 6.17 cm<sup>3</sup> K mol<sup>-1</sup> at 50 K and then increases to a peak value of 6.64 cm<sup>3</sup> K mol<sup>-1</sup> at 8.0 K, before decreasing very slightly to 6.51 cm<sup>3</sup> K mol<sup>-1</sup> at 5.0 K (Fig. 2, top). The value at 300 K is smaller than the spin-only ( $g = 2$ ) value of 9.75 cm<sup>3</sup> K mol<sup>-1</sup> for two Mn<sup>IV</sup> and two Mn<sup>III</sup> non-interacting ions, indicating dominant AF interactions within the Mn<sub>4</sub> unit (Table 4). The  $\chi_M T$  at the lowest temperatures suggests an  $S = 3$  or 4 ground state.



Scheme 1. .

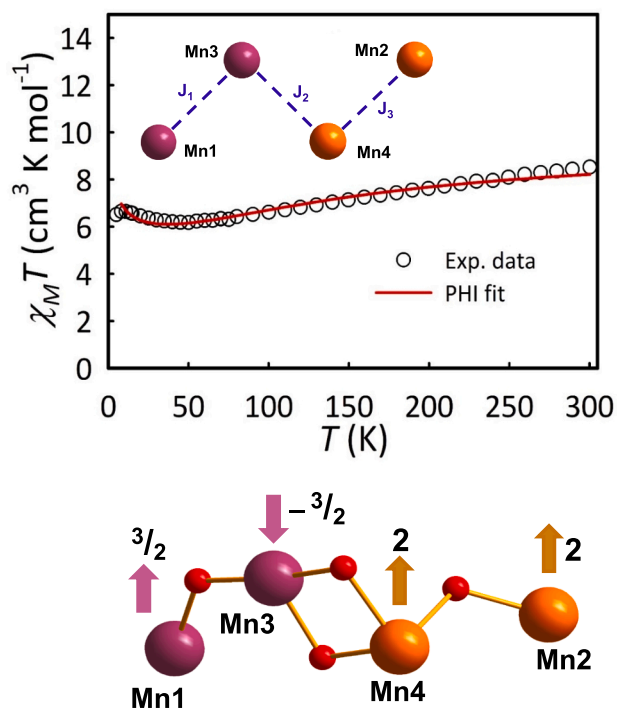


Fig. 2. (top)  $\chi_M T$  vs  $T$  data for 1·H<sub>2</sub>O. The red solid line is the fit of the data using program PHI to the 3- $J$  exchange coupling model shown as an inset; see the text for the fit parameters. (bottom) The Mn<sub>4</sub> unit showing the bridging O<sup>2-</sup> ions and the spin vector alignments in the  $S = 4$  ground state.

Table 4  
 $\chi_M T$  values for complexes 1·H<sub>2</sub>O – 4·H<sub>2</sub>O.

Compounds	Ln/Y free ion term	Calc $\chi_M T$ of Ln/Y free ion <sup>a</sup>	Exptl $\chi_M T$ at 5.0 K <sup>a</sup>	Exptl $\chi_M T$ at 300 K <sup>a</sup>	Calc $\chi_M T$ <sup>a,b</sup>
[Y <sub>9</sub> Mn <sub>4</sub> ] (1)	<sup>1</sup> S <sub>0</sub>	0	6.51	8.52	9.75
[Gd <sub>9</sub> Mn <sub>4</sub> ] (2)	<sup>8</sup> S <sub>7/2</sub>	7.9	139.54	66.80	80.85
[Tb <sub>9</sub> Mn <sub>4</sub> ] (3)	<sup>7</sup> F <sub>6</sub>	11.8	164.46	106.73	115.95
[Dy <sub>9</sub> Mn <sub>4</sub> ] (4)	<sup>6</sup> H <sub>15/2</sub>	14.2	159.07	119.22	137.55

<sup>a</sup> Units: cm<sup>3</sup> K mol<sup>-1</sup>.

<sup>b</sup> For non-interacting Mn<sup>III</sup><sub>2</sub>Mn<sup>IV</sup><sub>2</sub>Ln(Y)<sup>III</sup><sub>9</sub> ions, with  $g = 2$  for Mn.

Attempts were made to obtain the ground state of Y<sub>9</sub>Mn<sub>4</sub> complex 1·H<sub>2</sub>O from fits of magnetization ( $M$ ) vs field ( $H$ ) and  $T$  data collected in dc fields up to 7 T in the 1.8–10 K range. The resulting reduced magnetization ( $M/N\mu_B$ ) vs  $H/T$  data (Fig. 3), where  $N$  is Avogadro's number and  $\mu_B$  is the Bohr magneton, were fit using the program MAGNET [66], which assumes only the ground state is populated, incorporates axial zero-field splitting (ZFS) and the Zeeman term, and carries out a full powder average. The corresponding spin Hamiltonian is given in Eq. (2), where  $\hat{S}_z$

$$H = D\hat{S}_z^2 + g\mu_B\mu_0\hat{S}_z \quad (2)$$

is the z-axis spin operator,  $g$  is the electronic  $g$  factor, and  $\mu_0$  is the vacuum permeability. However, no satisfactory fit could be obtained. A common reason for this is low-lying excited states from weak coupling and/or spin frustration effects, and therefore data collected at higher fields were progressively excluded, a common way to mollify such problems. Using only data collected up to 1 T, a reasonable looking fit was obtained for  $S = 4$  (solid lines in Fig. 3) but with unreasonable  $g =$

1.61(2) and  $D = -0.24(2)$  cm<sup>-1</sup>. Another unreasonable fit was obtained for  $S = 3$  with  $g = 2.08(2)$  and  $D = -0.39(2)$  cm<sup>-1</sup> (solid lines in Fig. S1). Since magnetization fits are not very sensitive to the sign of  $D$ , we also identified the fits with  $D > 0$  from the  $D$  vs  $g$  error surfaces generated using program GRID [74], but these fits were also unreasonable (Fig. S2). We were surprised with these failures given the low Mn<sub>4</sub> nuclearity of the paramagnetic unit within 1, its 1-D zig-zag structure that precludes spin frustration effects, and the absence of Mn<sup>II</sup> that almost always gives weak couplings. Nevertheless, we suspected that the fit problems were due to the presence of some very weak couplings and the resultant presence of very low-lying excited states. To probe this further required fitting the  $\chi_M T$  vs  $T$  data to obtain the constituent  $J$  exchange couplings between Mn ions.

The Heisenberg spin Hamiltonian describing the exchange interactions within the zig-zag Mn<sub>4</sub> unit in 1·H<sub>2</sub>O (inset to Fig. 2, top) is given by Eq. (3), where  $S_1 = S_3 = 3/2$  for the Mn<sup>IV</sup> ions Mn1 and Mn3, and  $S_2 = S_4 = 2$  for the Mn<sup>III</sup> ions Mn2 and Mn4. The  $\chi_M T$  vs  $T$  data were fit to this 3- $J$

$$H = -2J_1\hat{S}_1\cdot\hat{S}_3 - 2J_2\hat{S}_3\cdot\hat{S}_4 - 2J_3\hat{S}_2\cdot\hat{S}_4 \quad (3)$$

model using program PHI [75], and a good fit was obtained with  $J_1 = -22.5(9)$  cm<sup>-1</sup>,  $J_2 = -7.6(5)$  cm<sup>-1</sup>, and  $J_3 = +0.30(3)$  cm<sup>-1</sup>, with a constant  $g = 1.97$  ( $g$  slightly less than 2, as expected for Mn<sup>III</sup>/Mn<sup>IV</sup>) and TIP =  $100 \times 10^{-6}$  cm<sup>3</sup> mol<sup>-1</sup> per Mn. The fit values predict an  $S_T = 4$  ground state with  $S_T = 3$  and  $S_T = 2$  excited states at 2.4 and 4.2 cm<sup>-1</sup>, respectively, above it. The very weak  $J_3$ , both in an absolute sense and relative to  $J_2$  and  $J_3$ , and the resultant very low-lying excited states rationalize the unsuccessful dc magnetization fits described above. It also allows the  $\chi_M T$  vs  $T$  plot to be dissected as follows: (i) at higher  $T$ , the antiferromagnetic (AF)  $J_1$  and  $J_2$  result in a steady decrease in  $\chi_M T$  with decreasing  $T$  reaching a minimum at 50 K of 6.17 cm<sup>3</sup>Kmol<sup>-1</sup>. This is consistent with the Mn<sub>3</sub> unit (Mn1/Mn3/Mn4) in an  $S = 2$  local ground state (Fig. 2, bottom) and negligible coupling with Mn2 ( $S = 2$ ); spin-only  $\chi_M T$  for two non-interacting  $S = 2$  units is 6.0 cm<sup>3</sup>Kmol<sup>-1</sup>. (ii) Below 50 K, the weak ferromagnetic (F)  $J_3$  begins to cause  $\chi_M T$  to increase, but the very low-lying excited states prevent it reaching the  $\sim 10$  cm<sup>3</sup>Kmol<sup>-1</sup> for the overall  $S_T = 4$  ground state shown in Fig. 2, bottom, giving instead a peak at 8.0 K of 6.64 cm<sup>3</sup>Kmol<sup>-1</sup> (for comparison, degenerate  $S = 2/S = 3/S = 4$  states give 7.0 cm<sup>3</sup>Kmol<sup>-1</sup> with  $g = 2$ ) and a decrease below 8.0 K as competing effects become apparent, likely weak intermolecular AF interactions through  $\pi/\pi$  stacking of mpko<sup>-</sup>chelates bound to Mn2. This dissection into two temperature regimes, above and below 50 K dominated by  $J_1/J_2$  and  $J_3$ , respectively, was supported by fitting only the 8.0 – 50 K data to two  $S = 2$  spins coupled by  $J_3$ , and this gave  $J_3 = +0.29(2)$  cm<sup>-1</sup> (Fig. S3), identical within uncertainty to that from the 3- $J$  model fit. This also provides support for  $J_3$  truly being very weakly F.

For 2·H<sub>2</sub>O to 4·H<sub>2</sub>O,  $\chi_M T$  remains almost constant in the 50 – 300 K range at  $\sim 66$ , 106 and 119 cm<sup>3</sup> K mol<sup>-1</sup> before increasing to 139.54, 164.46 and 159.07 cm<sup>3</sup> K mol<sup>-1</sup> at 5.0 K, respectively. The 300 K values are very approximately those for 9 Ln and 4 Mn non-interacting ions (Table 4 and Fig. 4). The overall profile is consistent with the expected weak Mn/Ln and Ln/Ln coupling, so that  $\chi_M T$  at  $T > 50$  K is roughly  $T$ -independent, and the steep increases at  $T < 50$  K are then indicative of predominantly F interactions or ferrimagnetic-like spin alignments from AF interactions, or both. Clearly, for such complicated, low-symmetry systems, it is difficult to deduce very much from the dc data, and additional insights were sought from ac susceptibility studies at very low  $T$ .

### 3.3.2. Ac magnetic susceptibility studies

The ac susceptibility data for 1·H<sub>2</sub>O to 4·H<sub>2</sub>O were collected in the 1.8–15 K range using a 3.5 G ac field at oscillation frequencies in the 50–1000 Hz range. For 1·H<sub>2</sub>O, the in-phase susceptibility ( $\chi'_M$ ), plotted as  $\chi'_M T$  in Fig. S4, is essentially constant at  $\sim 7$  cm<sup>3</sup> K mol<sup>-1</sup> in the 6–15 K range before decreasing at lower  $T$ , and there is no out-of-phase  $\chi''_M$

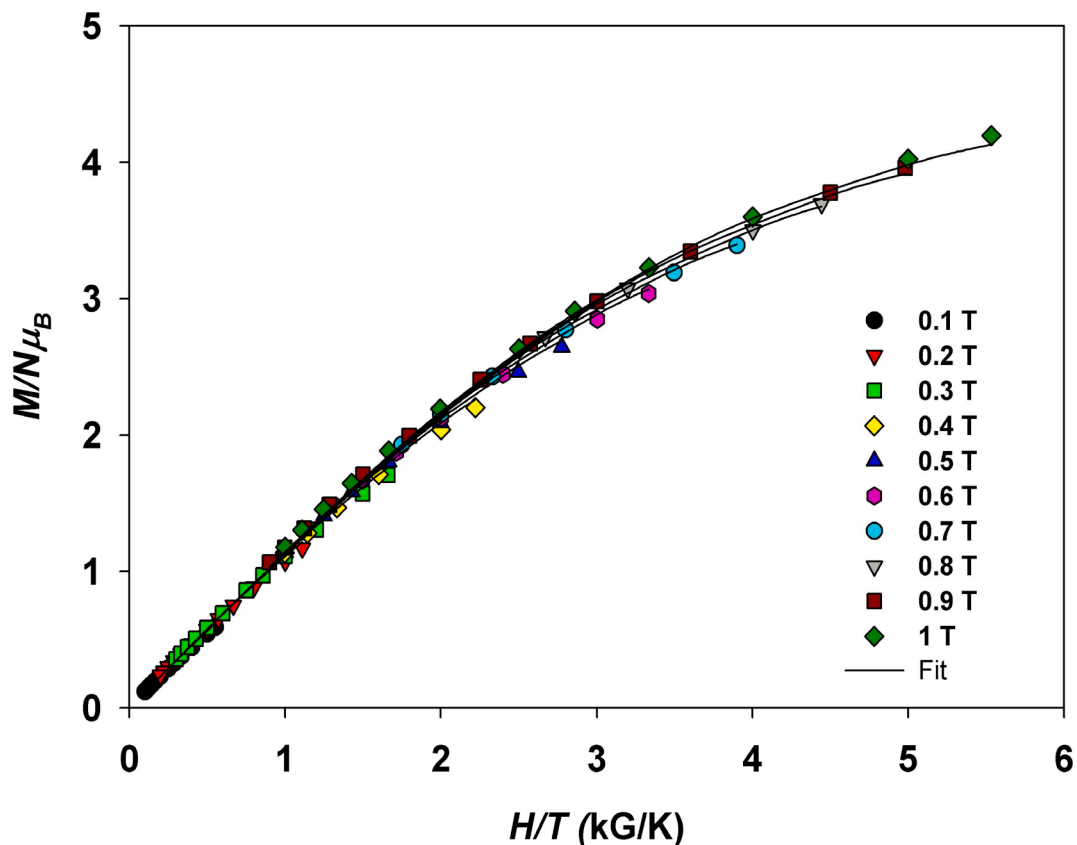


Fig. 3. Reduced magnetization ( $M/N\mu_B$ ) vs  $H/T$  plots for  $Y_9Mn_4$  complex  $1 \cdot H_2O$  for  $S = 4$  at the indicated applied fields. The solid lines are the fit of the data; see the text for the fit parameters.

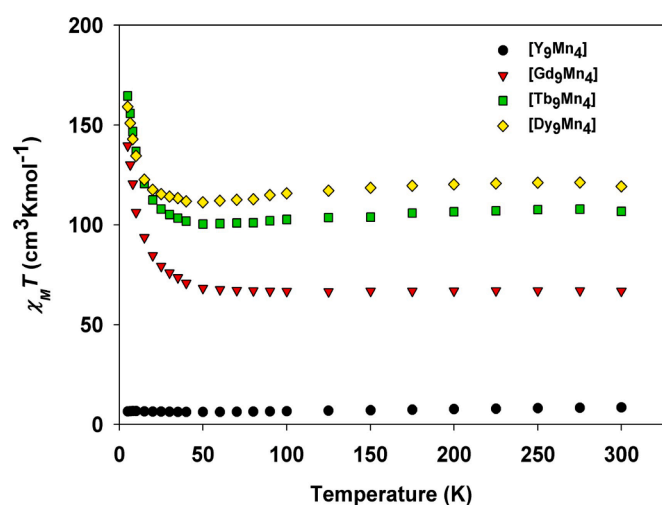


Fig. 4.  $\chi_M T$  vs  $T$  plots for  $\{Ln_9Mn_4\}$  complexes  $2 \cdot H_2O$  (Gd),  $3 \cdot H_2O$  (Tb), and  $4 \cdot H_2O$  (Dy) in a 0.1 T (1 kG) dc field, and comparison with the plot for  $1 \cdot H_2O$  (Y).

signal. For  $2 \cdot H_2O$ , which contains isotropic  $Gd^{III}$  ( $S = 7/2$ ), the in-phase  $\chi'_M T$  vs  $T$  plot (Fig. 5) shows a steep increase with decreasing  $T$  from  $96.27 cm^3 K mol^{-1}$  at 15 K to a plateau value of  $\sim 174 cm^3 K mol^{-1}$  at 1.8 K indicating a very high density of low-lying excited states with a smaller  $S$  than the ground state and an  $S = 18$  or 19 ground state. No  $\chi''_M$  signal was observed for  $2 \cdot H_2O$  (Fig. S5).

Increasing  $\chi'_M T$  with decreasing  $T$  below 50 K is also observed for  $3 \cdot H_2O$  (Fig. S6) and  $4 \cdot H_2O$  (Fig. 6) containing anisotropic  $Tb^{III}$  and  $Dy^{III}$ ,

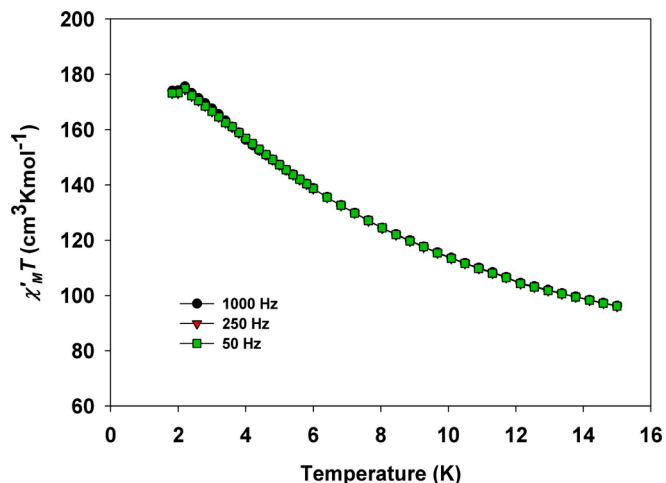


Fig. 5. Plot of ac in-phase susceptibility ( $\chi'_M$ , as  $\chi'_M T$ ) vs  $T$  for  $Gd_9Mn_4$  complex  $2 \cdot H_2O$  in the 1.8–15 K range. The solid line is a guide to the eyes.

respectively.  $\chi'_M T$  for the latter increases steeply below 15 K and is clearly heading to a value  $> 200 cm^3 K mol^{-1}$  at 0 K but then exhibits a frequency-dependent decrease in the 2–4 K region characteristic of the onset of slow relaxation of an SMM. As expected, there is a concomitant frequency-dependent  $\chi''_M$  appearing in the same temperature range (Fig. 6). The same  $\chi'_M T$  and  $\chi''_M$  profiles with decreasing  $T$  are seen for  $Tb_9Mn_4$  complex  $3 \cdot H_2O$  (Fig. S6) except that the frequency-dependent effects occur at lower  $T$ , indicating a smaller anisotropy barrier in  $3 \cdot H_2O$  vs  $4 \cdot H_2O$ .

Because no  $\chi''_M$  signals were observed in  $1 \cdot H_2O$  and  $2 \cdot H_2O$ , the SMM

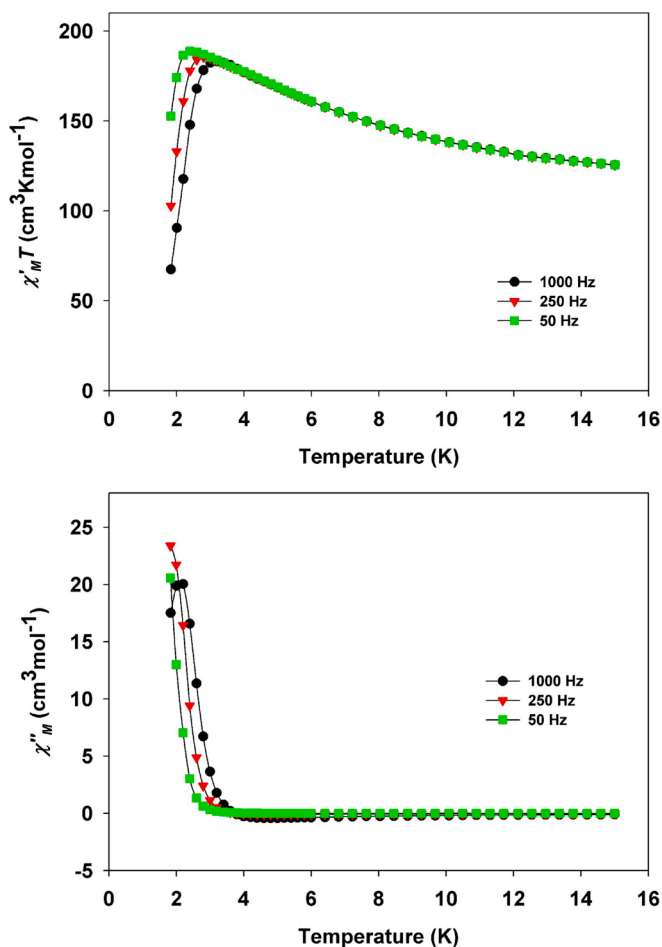


Fig. 6. The ac susceptibility in-phase  $\chi'_{M} T$  vs  $T$  (top) and out-of-phase  $\chi''_{M}$  vs  $T$  (bottom) plots for  $\text{Dy}_9\text{Mn}_4$  complex  $4\cdot\text{H}_2\text{O}$  in the 1.8–15 K range. The solid lines are guides to the eyes.

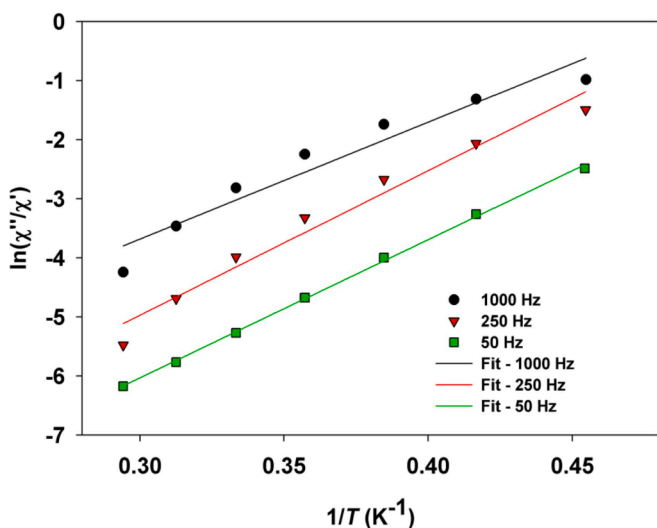


Fig. 7. Plot of  $\ln(\chi''_{M}/\chi'_{M})$  vs  $1/T$  for  $4\cdot\text{H}_2\text{O}$  at the indicated frequencies. The solid lines are the fit; see the text for the fit parameters.

behavior of  $3\cdot\text{H}_2\text{O}$  and  $4\cdot\text{H}_2\text{O}$  are solely attributed to the significant single-ion anisotropies of  $\text{Tb}^{\text{III}}$  and  $\text{Dy}^{\text{III}}$  ions. To roughly estimate the effective anisotropy barrier ( $U_{\text{eff}}$ ) of  $4\cdot\text{H}_2\text{O}$ , we employed Eq. (4), based on the

$$\ln(\chi''/\chi') = \ln(\omega\tau_0) + U_{\text{eff}}/k_{\text{B}}T \quad (4)$$

Kramers-Kronig equations [76], where  $\tau_0$  is the pre-exponential factor of the Arrhenius equation,  $k_{\text{B}}$  is the Boltzmann constant, and  $\omega$  is the angular frequency ( $2\pi f$ ) of the ac field. The resulting data and their fit to Eq. (4) (Fig. 7) have afforded  $U_{\text{eff}} = 16(1) \text{ cm}^{-1}$  and  $\tau_0 = 7(3) \times 10^{-9} \text{ s}$ . The small  $U_{\text{eff}}$  is consistent with the  $\chi''$  vs  $T$  plot, which shows signals only at very low  $T$ .

#### 4. Conclusions

The reaction of  $\text{Mn}(\text{O}_2\text{CPh})_2$  with  $\text{Y}^{\text{III}}$  or  $\text{Ln}^{\text{III}}$  salts and mpkoH in basic solution has provided access to a new family of 3d/4f clusters of nuclearity  $\text{Ln}_9\text{Mn}_4$  ( $\text{Ln} = \text{Gd}, \text{Tb}, \text{Dy}$ ) and  $\text{Y}_9\text{Mn}_4$ , facilitated by the well-recognized ability of mpko $^-$  to both chelate and bridge two or more metal ions. The  $\text{Y}_9\text{Mn}_4$  analogue has allowed the magnetic properties of the zig-zag  $\text{Mn}_4$  chain to be characterized as having an  $S = 4$  ground state, with the very weak  $F J_3$  ( $+0.30 \text{ cm}^{-1}$ ) aligning the two  $S = 2$  spin vectors parallel, but it would be inappropriate to assume that the same situation is present in the  $\text{Ln}_9\text{Mn}_4$  analogues since the Ln/Mn interactions would be of comparable magnitude to  $J_3$  and some would be competing with  $J_3$  unless they were all also F, which seems unlikely in such a high nuclearity low-symmetry complex. As stated above, the more likely situation is that there is a mixture of F and AF couplings in the clusters, and we note that all the Ln ions are bridged to the Mn ions by at least two  $\text{O}^{2-}/\text{OH}^-$  ions, except Mn2, so AF Ln/Mn couplings could be giving ferrimagnetic Ln/Mn/Ln alignments in parts of the molecule and a reasonable resultant ground state spin for the  $\text{Gd}_9\text{Mn}_4$  complex  $2\cdot\text{H}_2\text{O}$  of  $S = 18$  or 19. The SMM behavior of  $4\cdot\text{H}_2\text{O}$  is, of course, poor by modern standards, and not surprising given the nature of the cluster.

#### Declaration of Competing Interest

The authors declare that they have no known competing financial interests or personal relationships that could have appeared to influence the work reported in this paper.

#### Acknowledgement

This work was supported by the National Science Foundation (CHE-1900321).

#### Appendix A. Supplementary data

Supplementary data to this article can be found online at <https://doi.org/10.1016/j.poly.2021.115462>.

#### References

- [1] S. Osa, T. Kido, N. Matsumoto, N. Re, A. Pochaba, J. Mrozinski, J. Am. Chem. Soc. 126 (2004) 420.
- [2] G. Christou, D. Gatteschi, D.N. Hendrickson, R. Sessoli, MRS Bull. 25 (2000) 66.
- [3] M. Holyńska, D. Premuzić, I.-R. Jeon, W. Wernsdorfer, R. Clérac, S. Dehnen, Chem. Eur. J. 17 (2011) 9605.
- [4] L. Pham, K.A. Abboud, W. Wernsdorfer, G. Christou, Polyhedron 66 (2013) 205.
- [5] M.L. Kahn, P. Lecante, M. Verelst, C. Mathonière, O. Kahn, Chem. Mater. 12 (2000) 3073.
- [6] A. Mishra, W. Wernsdorfer, S. Parsons, G. Christou, E.K. Brechin, Chem. Commun. (2005) 2086.
- [7] C. Papatrifafllopoulou, K.A. Abboud, G. Christou, Inorg. Chem. 50 (2011) 8959.
- [8] C.G. Efthymiou, T.C. Stamatatos, C. Papatrifafllopoulou, A.J. Tasiopoulos, W. Wernsdorfer, S.P. Perlepes, G. Christou, Inorg. Chem. 49 (2010) 9737.
- [9] Y.-F. Zeng, G.-C. Xu, X. Hu, Z. Chen, X.-H. Bu, S. Gao, E.C. Sañudo, Inorg. Chem. 49 (2010) 9734.
- [10] H.-Z. Kou, S. Gao, X. Jin, Inorg. Chem. 40 (2001) 6295.
- [11] J.-P. Costes, F. Dahan, W. Wernsdorfer, Inorg. Chem. 45 (2005) 5.
- [12] M. Estrader, J. Ribas, V. Tangoulis, X. Solans, M. Font-Bardía, M. Maestro, C. Diaz, Inorg. Chem. 45 (2006) 8239.
- [13] S. Nayak, O. Roubeau, S.J. Teat, C.M. Beavers, P. Gamez, J. Reedijk, Inorg. Chem. 49 (2009) 216.

- [14] M.N. Akhtar, V. Mereacre, G. Novitchi, J.-P. Tuchagues, C.E. Anson, A.K. Powell, *Chem. Eur. J.* 15 (2009) 7278.
- [15] M. Murugesu, A. Mishra, W. Wernsdorfer, K.A. Abboud, G. Christou, *Polyhedron* 25 (2006) 613.
- [16] M. Ferbinteanu, T. Kajiwara, K.-Y. Choi, H. Nojiri, A. Nakamoto, N. Kojima, F. Cimpoesu, Y. Fujimura, S. Takaishi, M. Yamashita, *J. Am. Chem. Soc.* 128 (2006) 9008.
- [17] A. Baniodeh, I.J. Hewitt, V. Mereacre, Y. Lan, G. Novitchi, C.E. Anson, A.K. Powell, *Dalton Trans.* 40 (2011) 4080.
- [18] J.S. Kanady, E.Y. Tsui, M. Day, T. Agapie, *Science* 333 (2011) 733.
- [19] J.-L. Liu, J.-Y. Wu, G.-Z. Huang, Y.-C. Chen, J.-H. Jia, L. Ungur, L.F. Chibotaru, X.-M. Chen, M.-L. Tong, *Sci. Rep.* 5 (2015) 16621.
- [20] C.J. Milios, A. Prescimone, A. Mishra, S. Parsons, W. Wernsdorfer, G. Christou, S. P. Perlepes, E.K. Brechin, *Chem. Commun.* 153 (2007).
- [21] C.J. Milios, V. Vinslava, W. Wernsdorfer, S. Moggach, S. Parsons, S.P. Perlepes, G. Christou, E.K. Brechin, *J. Am. Chem. Soc.* 129 (2007) 2754.
- [22] T.C. Stamatatos, K.A. Abboud, W. Wernsdorfer, G. Christou, *Angew. Chem. Int. Ed.* 46 (2007) 902.
- [23] L.F. Jones, G. Rajaraman, J. Brockman, M. Murugesu, E.C. Sanudo, J. Raftery, S. J. Teat, W. Wernsdorfer, G. Christou, E.K. Brechin, D. Collison, *Eur. J. Chem.* 10 (2004) 5180.
- [24] A.J. Tasiopoulos, A. Vinslava, W. Wernsdorfer, K.A. Abboud, G. Christou, *Angew. Chem. Int. Ed.* 43 (2004) 2043.
- [25] A. Saha, M. Thompson, K.A. Abboud, W. Wernsdorfer, G. Christou, *Inorg. Chem.* 50 (2011) 10476.
- [26] G. Karotsis, S. Kennedy, S.J. Teat, C.M. Beavers, D.A. Fowler, J.J. Morales, M. Evangelisti, S.J. Dalgarno, E.K. Brechin, *J. Am. Chem. Soc.* 132 (2010) 12983.
- [27] H. Chen, C.-B. Ma, M.-Q. Hu, H.-M. Wen, H.-H. Cui, J.-Y. Liu, X.-W. Song, C.-N. Chen, *Dalton Trans.* 42 (2013) 4908.
- [28] A. Mishra, W. Wernsdorfer, K.A. Abboud, G. Christou, *J. Am. Chem. Soc.* 126 (2004) 15648.
- [29] C.M. Zaleski, E.C. Depperman, J.W. Kampf, M.L. Kirk, V.L. Pecoraro, *Angew. Chem. Int. Ed. Engl.* 43 (2004) 3912.
- [30] V.M. Mereacre, A.M. Ako, R. Clérac, W. Wernsdorfer, G. Filoti, J. Bartolomé, C. E. Anson, A.K. Powell, *J. Am. Chem. Soc.* 129 (2007) 9248.
- [31] T.C. Stamatatos, S.J. Teat, W. Wernsdorfer, G. Christou, *Angew. Chem. Int. Ed.* 48 (2009) 521.
- [32] A.M. Ako, V. Mereacre, R. Clerac, W. Wernsdorfer, I.J. Hewitt, C.E. Anson, A. K. Powell, *Chem. Commun.* (2009) 544.
- [33] C. Papatriantafyllopoulou, W. Wernsdorfer, K.A. Abboud, G. Christou, *Inorg. Chem.* 50 (2011) 421.
- [34] J.-L. Liu, W.-Q. Lin, Y.-C. Chen, J.-D. Leng, F.-S. Guo, M.-L. Tong, *Inorg. Chem.* 52 (2013) 457.
- [35] L. Pham, K.A. Abboud, W. Wernsdorfer, G. Christou, *Polyhedron* 155 (2018) 34.
- [36] R. Bagai, K.A. Abboud, W. Wernsdorfer, G. Christou, *Polyhedron* 142 (2018) 49.
- [37] A. Vinslava, A.J. Tasiopoulos, W. Wernsdorfer, K.A. Abboud, G. Christou, *Inorg. Chem.* 55 (2016) 3419.
- [38] A.J. Tasiopoulos, T.A. O'Brien, K.A. Abboud, G. Christou, *Angew. Chem. Int. Ed.* 43 (2004) 345.
- [39] (a) A.J. Tasiopoulos, W. Wernsdorfer, K.A. Abboud, G. Christou, *Inorg. Chem.* 44 (2005) 6324; (b) A.J. Tasiopoulos, W. Wernsdorfer, K.A. Abboud, G. Christou, *Polyhedron* 24 (2005) 2505; (c) S. Wang, K. Foltling, W.E. Streib, E.A. Schmitt, J.K. McCusker, D. N. Hendrickson, G. Christou, *Angew. Chem. Int. Ed. Engl.* 30 (1991) 305.
- [40] R. Sessoli, A.K. Powell, *Coord. Chem. Rev.* 253 (2009) 2328.
- [41] S.D. Gupta, R. Steward, D.-T. Chen, K. Aboud, H.-P. Cheng, S. Hill, G. Christou, *Inorg. Chem.* 59 (2020) 8716.
- [42] (a) L.R. Piquer, E.C. Sanudo, *Dalton Trans.* 44 (2015) 8771; (b) C.G. Efthymiou, T.C. Stamatatos, C. Papatriantafyllopoulou, A.J. Tasiopoulos, W. Wernsdorfer, S.P. Perlepes, G. Christou, *Inorg. Chem.* 49 (2010) 9737.
- [43] H.-S. Wang, K. Zhang, Y. Song, Z.-Q. Pan, *Inorg. Chim. Acta* 521 (2021), 120318.
- [44] D. Burdinski, F. Birkelbach, T. Weyhermüller, U. Flörke, H.-J. Haupt, M. Lengen, A. X. Trautwein, E. Bill, K. Wieghardt, P. Chaudhuri, *Inorg. Chem.* 37 (1998) 1009.
- [45] P. Chaudhuri, *Coord. Chem. Rev.* 243 (2003) 143.
- [46] P. Chaudhuri, M. Hess, T. Weyhermüller, E. Bill, H.-J. Haupt, U. Flörke, *Inorg. Chem. Commun.* 1 (1998) 39.
- [47] P. Chaudhuri, M. Winter, F. Birkelbach, P. Fleischhauer, W. Haase, U. Floerke, H. J. Haupt, *J. Inorg. Chem.* 30 (1991) 4291.
- [48] C.J. Milios, T.C. Stamatatos, S.P. Perlepes, *Polyhedron* 25 (2006) 134.
- [49] H. Miyasaka, R. Clerac, *Bull. Chem. Soc. Jpn.* 78 (2005) 1725.
- [50] F. Mori, T. Nyui, T. Ishida, T. Nogami, K.-Y. Choi, H. Nojiri, *J. Am. Chem. Soc.* 128 (2006) 1440.
- [51] J.M. Thorpe, R.L. Beddoes, D. Collison, C.D. Garner, M. Helliwell, J.M. Holmes, P. A. Tasker, *Angew. Chem. Int. Ed.* 38 (1999) 1119.
- [52] I.F. Jones, A. Prescimone, M. Evangelisti, E.K. Brechin, *Chem. Commun.* (2009) 2023.
- [53] C. Efthymiou, I. Mylonas-Margartitis, S. Gupta, A. Tasiopoulos, V. Nastopoulos, G. Christou, S. Perlepes, C. Papatriantafyllopoulou, *Polyhedron* 171 (2019) 330.
- [54] C. Stoumpos, T. Stamatatos, H. Sartz, O. Roubeau, A. Tasiopoulos, V. Nastopoulos, S. Teat, G. Christou, S. Perlepes, *Dalton Trans.* 6 (2009) 1004.
- [55] C.D. Polyzou, H. Nikolaou, C. Papatriantafyllopoulou, V. Psycharis, C. P. Raptopoulou, A. Escuer, S.P. Perlepes, *Dalton Trans.* 41 (2012) 13755.
- [56] F. Martinez, C. Bazzicalupi, A. Bianchi, F. Lloret, R. Gonzalez, C. Kremer, R. Chiozzone, *Polyhedron* 138 (2017) 125.
- [57] L. Martinez, L. Arizaga, D. Armentano, F. Lloret, R. Gonzalez, C. Kremer, R. Chiozzone, *J. Coord. Chem.* 71 (2018) 748.
- [58] T. Ghosh, K.A. Abboud, G. Christou, *Polyhedron* 173 (2019), 114145.
- [59] T.C. Stamatatos, D. Foguet-Albiol, S.-C. Lee, C.C. Stoumpos, C.P. Raptopoulou, A. Terzis, W. Wernsdorfer, S.O. Hill, S.P. Perlepes, G. Christou, *J. Am. Chem. Soc.* 129 (2007) 9484.
- [60] (a) T.N. Nguyen, M. Shiddiq, T. Ghosh, K.A. Abboud, S. Hill, G. Christou, *J. Am. Chem. Soc.* 137 (2015) 7160; (b) T.N. Nguyen, W. Wernsdorfer, K.A. Abboud, G. Christou, *J. Am. Chem. Soc.* 133 (2011) 20688; (c) T. Ghosh, J. Marbey, W. Wernsdorfer, S. Hill, K.A. Abboud, G. Christou, *Phys. Chem. Chem. Phys.* 23 (2011) 8854.
- [61] A.M. Mowson, T.N. Nguyen, K.A. Abboud, G. Christou, *Inorg. Chem.* 52 (2013) 12320.
- [62] O.A. Adebayo, K.A. Abboud, G. Christou, *Polyhedron* 122 (2017) 71.
- [63] O.A. Adebayo, K.A. Abboud, G. Christou, *Inorg. Chem.* 56 (2017) 11352.
- [64] SAINT (2013) Bruker-AXS, Madison, Wisconsin, USA.
- [65] (a) SHELXTL2013 (2013). Bruker-AXS, Madison, Wisconsin, USA. (b) P. Van Der Sluis, A.L. Spek. *Acta Crystallogr. A* 46 (1990) 194. (c) A.L. Spek. *Acta Crystallogr. C* 71 (2015) 9.
- [66] MAGNET. E. R. Davidson, Indiana University, Bloomington, IN (1999).
- [67] N.E. Breese, M. O'Keeffe, *Acta Cryst.* B47 (1991) 192.
- [68] G.J. Palenik, *Inorg. Chem.* 36 (1997) 4888.
- [69] A. Gupta, R.K. Sharma, R. Bohra, V.K. Jain, J.D. Drake, M.B. Hursthouse, M. E. Light, *Polyhedron* 21 (2002) 2387.
- [70] T.C. Stamatatos, A. Bell, P. Cooper, A. Terzis, C.P. Raptopoulou, S.L. Heath, R.E. P. Winpenny, S.P. Perlepes, *Inorg. Chem. Commun.* 8 (2005) 533.
- [71] V. Sharma, R.K. Sharma, R. Bohra, R. Ratnani, V.K. Jain, J.E. Drake, M. B. Hursthouse, M.E. Light, *J. Organomet. Chem.* 651 (2002) 98.
- [72] V. Sharma, R.K. Sharma, R. Bohra, K. Jain, J.E. Drake, M.E. Light, M.B. Hursthouse, *J. Organomet. Chem.* 664 (2002) 66.
- [73] C. Papatriantafyllopoulou, G. Aromi, A.J. Tasiopoulos, V. Nastopoulos, C. P. Raptopoulou, S.J. Teat, A. Escuer, S.P. Perlepes, *Eur. J. Inorg. Chem.* 2007 (2007) 2761.
- [74] GRID Indiana University, Bloomington, IN, 1999.
- [75] N.F. Chilton, R.P. Anderson, L.D. Turner, A. Soncini, K.S. Murray, *J. Comput. Chem.* 34 (2013) 1164.
- [76] J. Bartolomé, G. Filoti, V. Kuncser, G. Schinteie, V. Mereacre, C.E. Anson, A. K. Powell, D. Prodius, C. Turta, *Phys. Rev. B* 80 (2009), 014430.